Bending and Uniaxial Tensile Tests on Concrete Reinforced with Hybrid Steel Fibers

L. G. Sorelli[1]; A. Meda[2]; and G. A. Plizzari[3]

Abstract: Based on the idea of taking simultaneous advantage of the effects of different types of fibers, new materials called hybrid fiber reinforced concretes have been developed by combining fibers of different geometry and material. In the present paper, the benefits in terms of concrete toughness from a combination of micro- and macrosteel fibers are evaluated under both bending and uniaxial tensile tests on specimens of different sizes. Experimental results are very sensitive to the strain gradient in the cracked section, to the fiber geometry and to the area of the cracked surface. In fact, a larger scatter in the experimental results was observed in specimens with smaller cracked surfaces where a greater variation of the macrofiber density occurred. For this reason, beside the size effects, the fiber size and the dimension of the cracked section markedly influence the characteristic value of the fracture parameters. A numerical simulation based on nonlinear fracture mechanics of the experimental test was carried out in order to better identify the fiber contribution in the fracture propagation.

DOI: 10.1061/(ASCE)0899-1561(2005)17:5(519)

CE Database subject headings: Fiber reinforced materials; Concrete; Steel fibers; Tensile strength; Fractures.

Introduction

The interest in concrete reinforced with fibers has continuously grown after Romualdi and Batson (1963) highlighted the possibility of obtaining concretes with enhanced properties (Shah and Rangan 1971; di Prisco et al. 2004). Fiber reinforced concrete (FRC) is presently used extensively in structures where the reinforcement is not essential for integrity and safety (e.g., slabs on grade, shotcrete in tunnels and light precast elements) but, recently, fibers have also been used as principal reinforcement in structures under bending and shear [e.g., precast prestressed beams, thin-web roof elements, and tunnel segments (Meda et al. 2002; di Prisco et al. 2003)]. Fibers for concrete are made of different materials and geometries and each type of fiber improves some specific concrete performances. Usually steel fibers are adopted to improve mechanical properties (toughness) whereas plastic fibers can reduce cracking due to shrinkage and avoid spalling phenomena in concrete under fire action.

Recently the idea of taking simultaneous advantage of the effects of different types of fibers has been explored and new materials, called hybrid FRCs, have been developed by combining fibers of differing geometry and/or material (Banthia et al. 2000; Banthia and Nandakumar 2003). As an example, Lawler et al. (2002) showed that a combination of fibers of different lengths improves both toughness and impermeability of the composite. Also from the mere mechanical point of view, synergistic effects were observed on the pull-out strength of a single steel fiber from a cementitious matrix reinforced with short steel fibers (Markovic et al. 2002).

Concrete toughness is better determined by performing uniaxial tensile tests but the experimental difficulties related to these tests suggested several code makers to propose bending tests instead (either with three or four point loading). Fracture tests are remarkably influenced by the strain gradient (Slowik and Wittmann 1992) and, when low volume fractions of steel fibers are adopted, experimental results are often characterized by a large scatter that reduces the characteristic values that are required for design purposes.

The aim of the present work is to investigate the possibility of optimizing concrete toughness by combining steel fibers of two different sizes. Concrete toughness was determined by means of both uniaxial and bending tests on notched specimens. Freely rotating platens with spherical hinges were adopted as boundary conditions in the uniaxial tests to better control the crack development. Bending tests were carried out on beam specimens having two different geometries and different notch length/beam depth ratios. One of the beam geometries had the same fracture

Table 1. Properties of Steel Fibers

Properties	Macrofiber	Microfiber
Length (L_f) (mm)	30	12
Diameter (ϕ_f) (mm)	0.60	0.18
Aspect ratio (L_f/ϕ_f)	50	67
Tensile strength (MPa)	1,100	1,800
Young's modulus (GPa)	210	210

[1]Research Assistant, Dept. of Civil Engineering, Univ. of Brescia, Via Branze 38, Brescia (BS), Italy.

[2]Assistant Professor, Dept. of Engineering Design and Technologies, Univ. of Bergamo, Viale Marconi 5, Dalmine (BG), I-24044, Italy.

[3]Professor, Dept. of Engineering Design and Technologies, Univ. of Bergamo, Viale Marconi 5, Dalmine (BG), I-24044, Italy.

Note. Associate Editor: Kiang-Hwee Tan. Discussion open until March 1, 2006. Separate discussions must be submitted for individual papers. To extend the closing date by one month, a written request must be filed with the ASCE Managing Editor. The manuscript for this paper was submitted for review and possible publication on February 23, 2004; approved on July 20, 2004. This paper is part of the ***Journal of Materials in Civil Engineering***, Vol. 17, No. 5, October 1, 2005. ©ASCE, ISSN 0899-1561/2005/5-519–527/$25.00.

Table 2. Fiber Combinations, Compressive Strength, and Workability (Slump) for the Concrete Adopted

Material	Steel fiber 30/0.6 $(\%)_{vol.}$	Steel fiber 12/0.18 $(\%)_{vol.}$	Total volume fraction $V_{f,tot}$ $(\%)_{vol.}$	Compressive strength $f_{c,cube}$ (MPa)	Slump s (mm)
Plain	—	—	—	28.3	150
Macrofiber	0.38	—	0.38	29.3	110
Microfiber	—	0.38	0.38	31.9	130
Hybrid	0.19	0.19	0.38	33.0	130

surface of the uni-axial specimens to better study the strain gradient effects (Slowik and Wittmann 1992).

Numerical simulations based on nonlinear fracture mechanics (Hillerborg et al. 1976) with a discrete crack approach were carried out in order to characterize the fracture properties of the material in a better way. The determination of a good approximation of the post-cracking behavior based on a polylinear law was investigated and the suitability of adopting a bilinear law (for concrete with a single type of fiber) and a trilinear law (for concrete with two types of fiber) has been studied. In fact, since fibers of different lengths become efficient at different stages of the cracking process, the smaller fibers control the microcrack growth whereas the longer fibers become active for larger crack openings.

Experiments

Materials

Experiments were carried out on specimens made of a normal strength concrete with 355 kg/m^3 of cement [CEM II/A-LL 32.5R according to UNI-EN 197 (CEN 2000)], 180 kg/m^3 of water (water-cement ratio of 0.55), 3.9 L/m^3 of superplasticiser, and 1,900 kg/m^3 of aggregates with a maximum size of 15 mm. A grain size distribution close to the Bolomey curve was used.

Two different types of steel fibers were adopted: the first one had a length (L_f) of 30 mm and a diameter (ϕ_f) of 0.6 mm whereas the second one was a shorter fiber having a length of 12 mm and a diameter of 0.18 mm; these fibers will be named as "macrofiber" and "microfiber," respectively. The geometrical and mechanical characteristics of the fibers used in the present work are reported in Table 1.

Fibers were added to the concrete matrix in four different combinations as shown in Table 2: one plain concrete and three concretes having a volume fraction of fibers often used in practice, equal to 0.38% (30 kg/m^3), in all cases. Table 2 also shows concrete compressive strength measured after 28 days of curing on cube specimens ($150\times150\times150$ mm) and the slump of the fresh concrete; the slight decrease of workability of FRC can be observed. The specimens were cured in a fog room until the time of the test and a vaseline layer was applied on the crack section in order to limit shrinkage cracking.

Experimental Setup

In order to investigate the fiber effects on concrete behavior, fracture tests should be performed and a stable control of the test is necessary. For this reason, a 500 kN hydraulic testing machine (Instron 8500+) with a proportional integrative derivative (PID) closed loop control that permits to compensate the finite stiffness of the load system was adopted. The crack mouth opening displacement (CMOD), measured by a clip gauge, was adopted as feedback signal in both the uniaxial and the bending tests.

Uniaxial tests with freely rotating platens were performed on specimens having a size of $100\times200\times40$ mm [Fig. 1(a)] that were sawn from concrete prisms having a size of $100\times200\times400$ mm to favor a three-dimensional distribution of the fibers. A single notch with a depth of 15 mm, a width of 4 mm and a tip with a triangular shape was sawn with a diamond blade. Four linear variable differential transducers (LVDTs) with a base length of 45 mm were located across the notched section to evaluate the relative displacement and rotation of the sections at each side of the crack surface [Fig. 1(a)]. In order to reduce undesired eccentricities, the specimens were carefully positioned (and then glued) on steel platens by adopting 4 instruments with a precision of 0.01 mm; this gave good alignment of the specimen along the loading axis [Fig. 1(b)]. The free rotation of the platens was obtained by means of two spherical hinges placed at 150 mm from

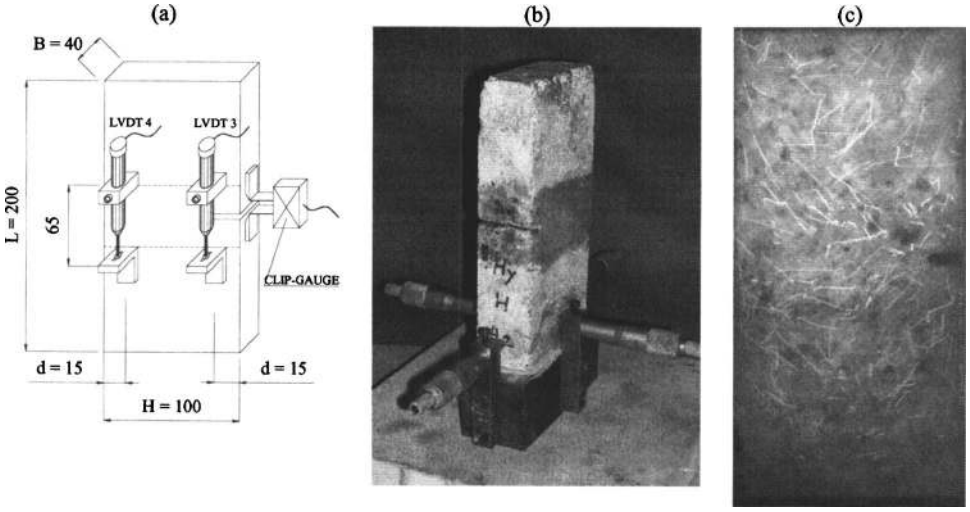

Fig. 1. (a) Tensile test specimen instrumented with four linear variable differential transducers and one clip gauge; (b) setup for positioning the steel platens; and (c) fiber distribution from a x-ray picture

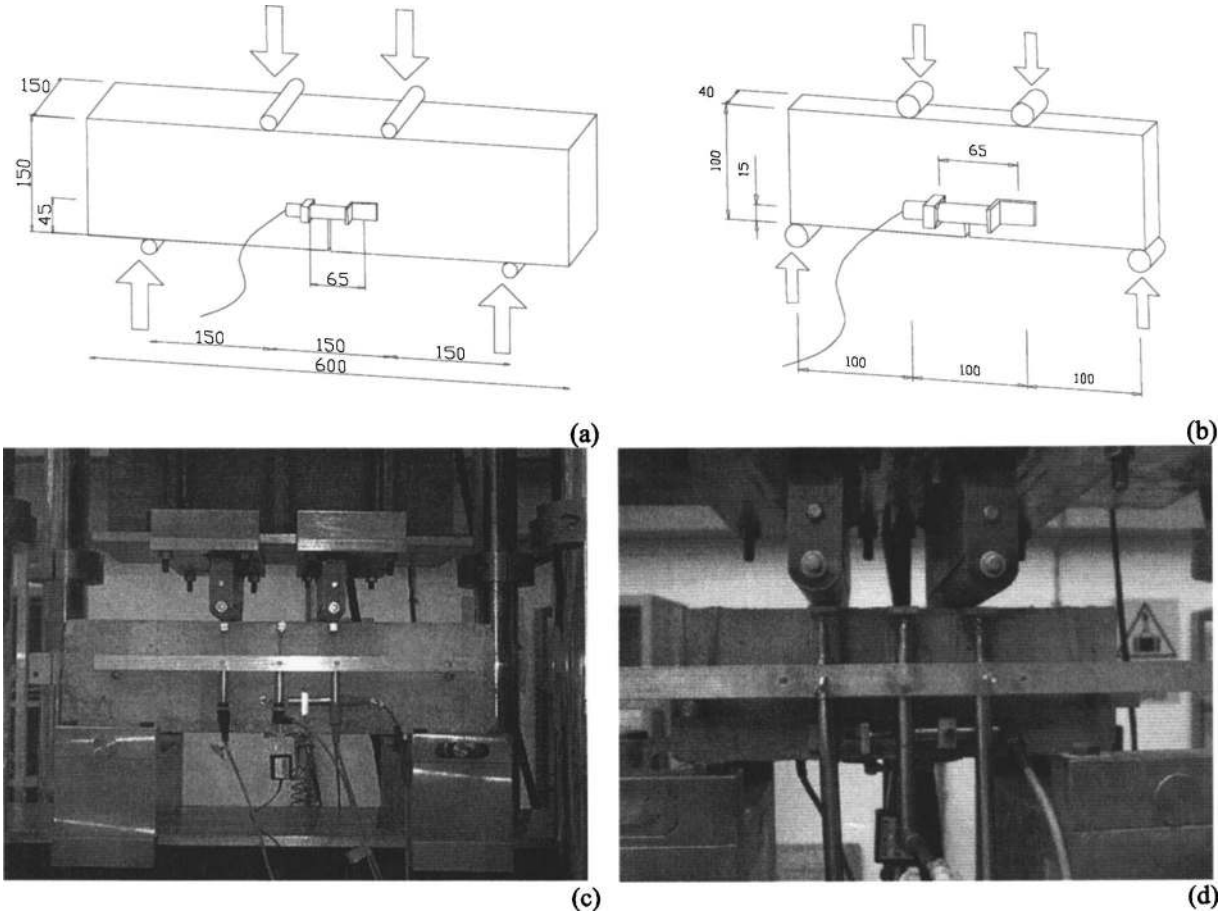

Fig. 2. (a, b) Specimen geometry and (c, d) testing setup for the larger and smaller beams, respectively

the glued surface: in this way it was possible to localize the center of rotation at the specimen ends. The tests were carried out by imposing a CMOD rate of 1 μm/min until the load–displacement curve had passed the peak and the fiber started activating. Afterwards, the CMOD rate was set to 2 μm/min. Although it includes the elastic deformations of concrete, the average value of the displacement measured by the two LVDTs astride the notch was conventionally assumed as the crack tip opening displacement (CTOD) [Fig. 1(a)]. The fiber distribution in a few specimens were checked before testing by means of x ray. From the x-ray image [Fig. 1(c)] it is possible to observe the random distribution of fibers with the shadows of the macrofibers and the faint traces of the microfibers.

Four point bending tests were performed on two different specimen sizes. The first one had a size of $150 \times 150 \times 600$ mm with a notch depth of 45 mm and was tested according to the Italian Standard [Fig. 2(a)] (UNI 2003). The second one had the same crack surface as the uniaxial tensile test specimen to study the strain gradient effects: these beams had a size of $100 \times 320 \times 40$ mm and were tested with a span length of 300 mm and a distance between the load points of 100 mm [Fig. 2(b)].

Three LVDTs were used to measure the vertical displacement at mid-span and under the load points whereas two LVDTs were placed at the notch tip to measure the CTOD [Figs. 2(c and d)]. Further, a clip gauge was placed across the notch to measure the CMOD [Fig. 2(c)]. The CMOD rate was 50 μm/min for the larger beams (UNI 2003) and 2.5 μm/min for the smaller beams.

Table 3. Average Number of Fibers Intercepted on the Crack Section with Indication of the Standard Deviation (in parentheses) for Each Test and Material

	Material			
			Hybrid	
Test	Macrofiber (macrofibers/cm^2)	Microfiber (microfibers/cm^2)	(macrofibers/cm^2)	(microfibers/cm^2)
Uniaxial	0.33 (±33%)	3.02 (±19%)	0.25 (±49%)	1.88 (±37%)
4PBT—small beams	0.68 (±30%)	3.43 (±9%)	0.35 (±33%)	1.85 (±9%)
4PBT—large beams	0.32 (±13%)	n.a.	0.22 (±15%)	n.a.
All tests	0.44	3.22*	0.27	1.86*

Note: 4PBT=four point bending test; n.a.=not available; and *=evaluated from the uniaxial tensile tests and the 4PBT on small beams.

Table 4. Average Nominal Strength with Indication of the Standard Deviation (in parentheses) for Each Test and Material

	Material			
Test	Plain (MPa)	Macrofiber (MPa)	Microfiber (MPa)	Hybrid (MPa)
Uniaxial	2.85 (±10%)	2.25 (±17%)	3.09 (±7%)	2.67 (±15%)
4PBT—small beams	3.29 (±15%)	3.28 (±11%)	3.67 (±7%)	3.83 (±7%)
4PBT—large beams	4.17 (±5%)	4.19 (±25%)	4.51 (±22%)	4.98 (±17%)

Note: 4PBT=four point bending test.

Results

In order to obtain a clearer comparison between the different specimen geometries, experimental results from the uni-axial tensile and bending tests are reported in terms of nominal stress (σ_N) defined according to a linear stress distribution as

$$\sigma_N = \frac{F}{B_s(H_s - a_0)} + \frac{Fa_0/2}{(1/6)B_s(H_s - a_0)^2} \tag{1}$$

for the uniaxial tensile test, where F=force; B_s and H_s =thickness and the height of the specimen respectively; and a_0 =notch depth [Fig. 1(a)].

For the four point bending test, the nominal stress is given by

$$\sigma_N = \frac{FL_{sp}}{B_b(H_b - a_0)^2} \tag{2}$$

where F=force; B_b and H_b=beam thickness and depth, respectively; L_{sp}=span length; and a_0=notch depth [Figs. 2(a and b)]. At least four specimens for each material and each specimen geometry were tested.

Experimental results from fiber reinforced concrete with low fiber contents are very sensitive to the number of fibers in the cracked sections which have a higher degree of variation in the smaller surface areas, especially when notched specimens are adopted. Table 3 reports the average value of the fiber density in the cracked surface (number of fibers in the crack surface per unit

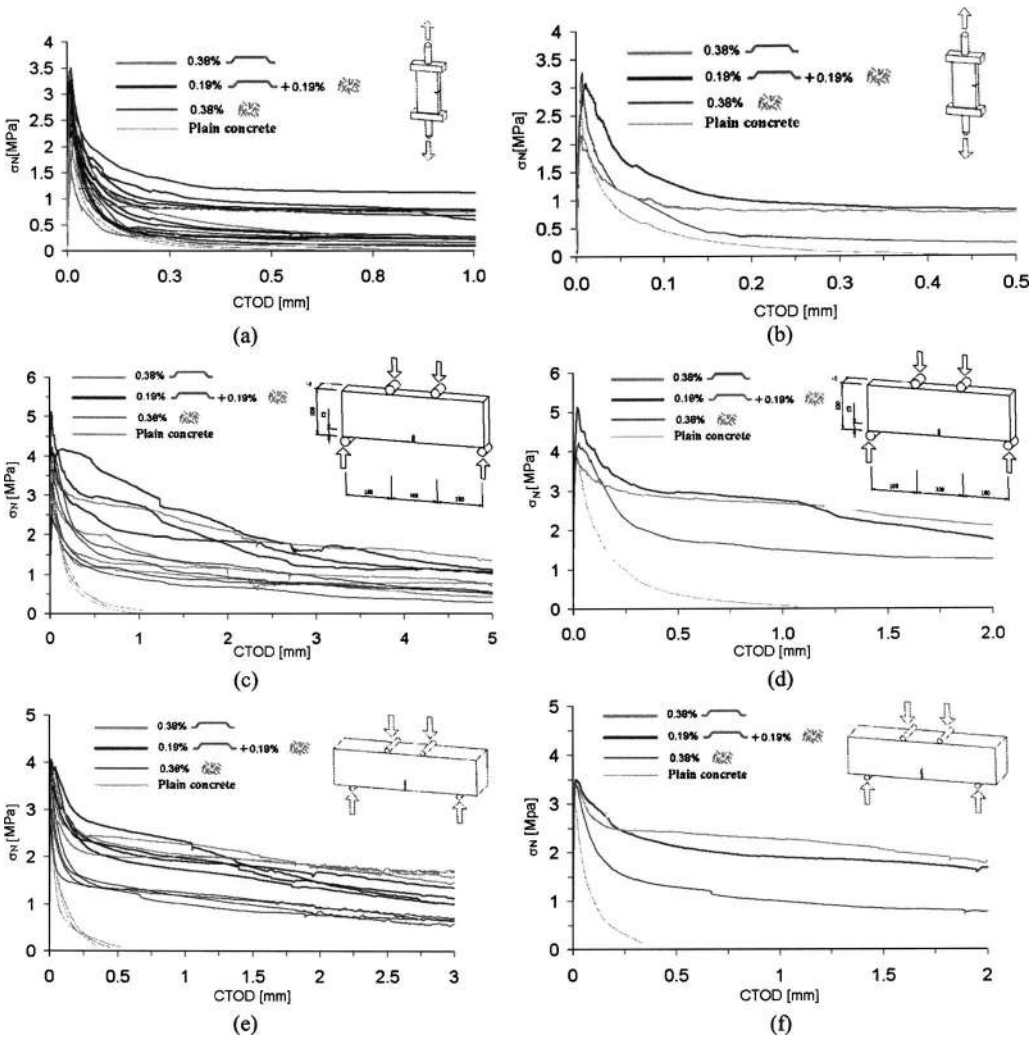

Fig. 3. Nominal stress versus crack tip opening displacement (CTOD) for (a, b) uni-axial tensile tests; (c, d) small bending tests; and (e, f) large bending tests for (left-hand side) all the specimens and (right-hand side) a selection of them

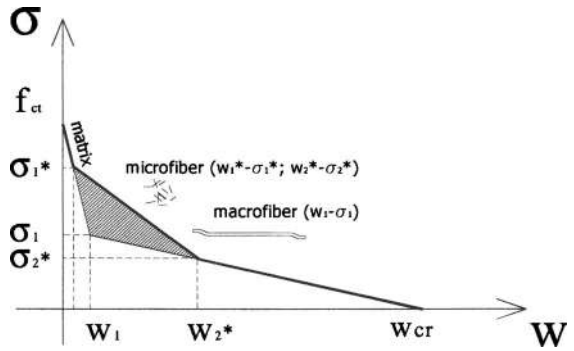

Fig. 4. Approximation of the softening law by a bilinear or trilinear curve

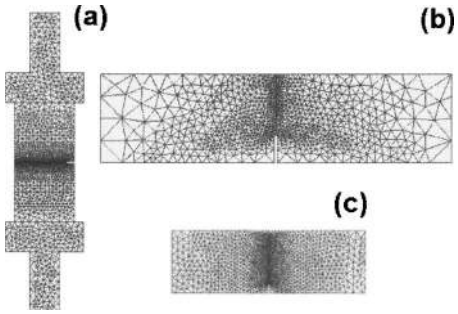

Fig. 5. Finite element meshes of the tensile specimen with (a) steel plates; (b) large beam specimens; and (c) small beam specimens

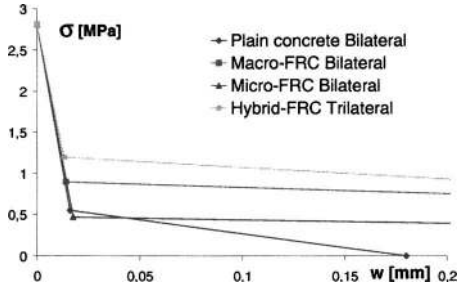

Fig. 6. Stress–crack opening curves determined from the best-fitting procedure

area) for each specimen type and material, as well as the standard deviation. Because of the larger fractured surface, it was not possible to count the number of microfibers in the larger beams. It will be noticed that the average density of macrofibers is around 0.3–0.4 fibers/cm^2 for both the uniaxial specimens and the larger beams and that larger fibers and smaller crack surfaces are characterized by a higher scatter in the fiber density. For this reason, in addition to the size effects, the dimensions of the fiber and the cracked section markedly influence the characteristic value of the fracture parameters. Specimens with microfibers are characterized by a lower variation of the fiber density; this is due to the greater number of microfibers that cross the cracked section with respect to the macrofibers; in these specimens, the standard deviation of the peak-load value is reduced (Table 4).

The scatter of the experimental results markedly influences the design values of the material properties, much more than in other

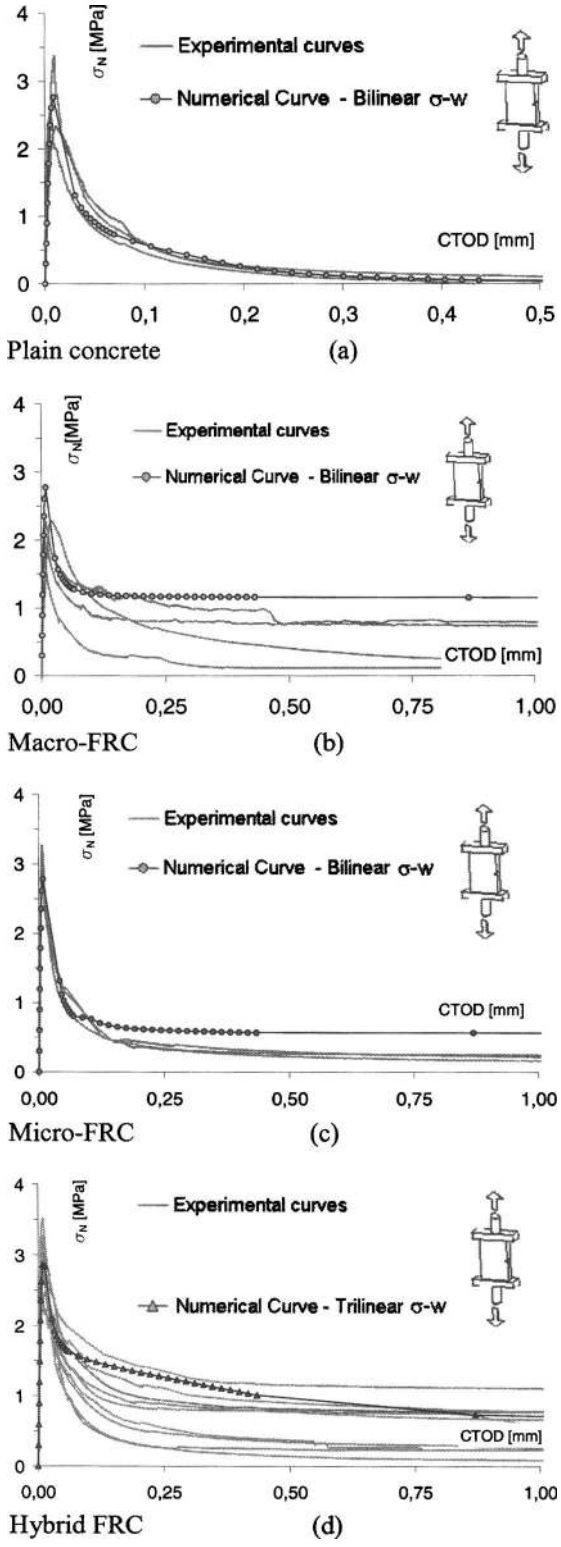

Fig. 7. Experimental and numerical nominal stress (σ_N) versus crack tip opening displacement (CTOD) curves from uniaxial tensile tests

structural materials. Since the scatter depends on the specimen size, which usually is much smaller than the structure, the design values for FRC should take the specimen size into account.

The left-hand side of Fig. 3 shows the nominal stress versus the CTOD obtained from tests on specimens with different geometries and made of different materials; one should remember that all the fiber reinforced specimens were characterized by the same

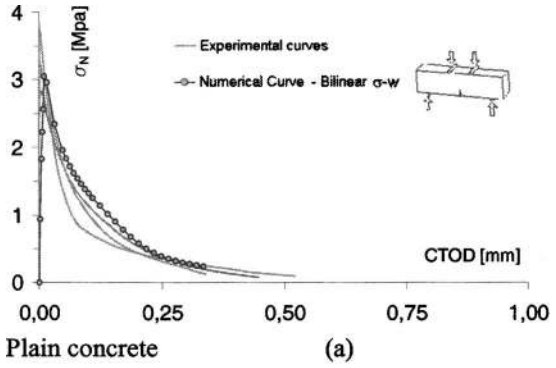

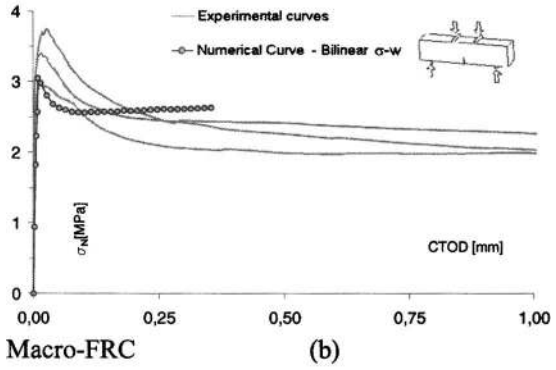

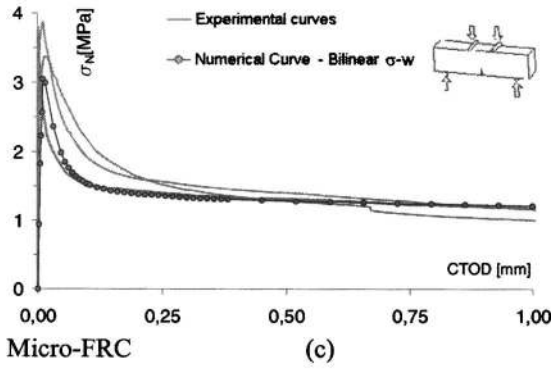

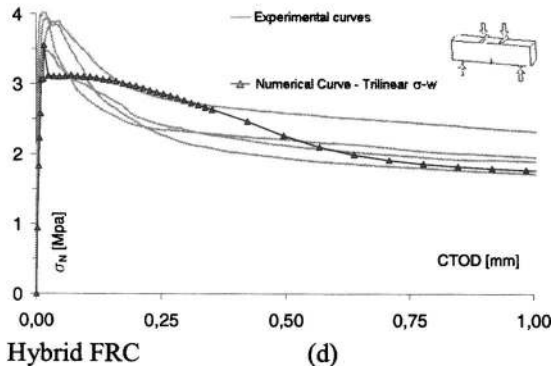

Fig. 8. Experimental and numerical nominal stress versus crack tip opening displacement (CTOD) for (a) plain concrete; (b) macro-FRC; (c) micro-FRC; and (d) hybrid FRC from bending tests on large specimens (note: FRC=fiber reinforced concrete)

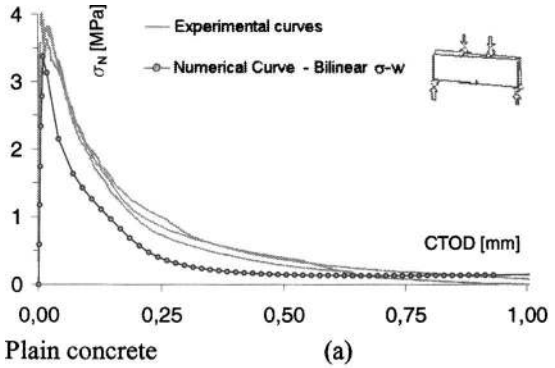

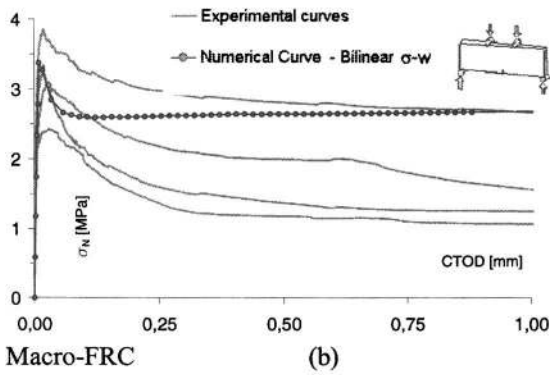

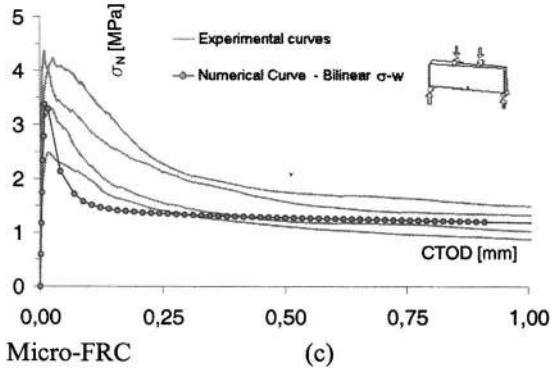

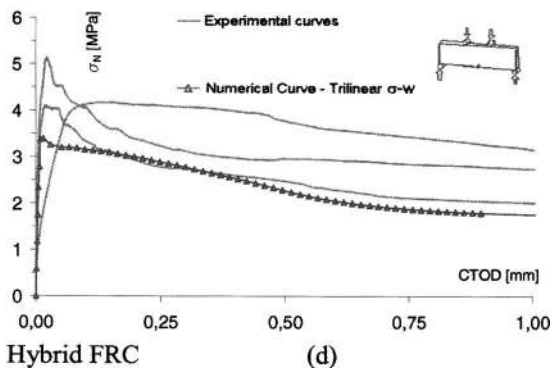

Fig. 9. Experimental and numerical nominal stress versus crack tip opening displacement for (a) plain concrete; (b) macro-FRC; (c) micro-FRC; and (d) hybrid FRC from bending tests on small specimens (note: FRC=fiber reinforced concrete)

Table 5. Constitutive Parameters for the $\sigma-w$ law (*trilinear relationship)

	f_{ct} (MPa)	σ_1 (MPa)	w_1 (mm)	σ_2 (MPa)	w_2 (mm)	w_{cr} (mm)
Plain concrete	2.81	0.55	0.016	—	—	0.18
Macro-FRC	2.81	0.90	0.014	—	—	50
Micro-FRC	2.81	0.47	0.0175	—	—	3
Hybrid-FRC*	2.81	1.20	0.013	0.50	0.50	50

Note: FRC=fiber reinforced concrete.

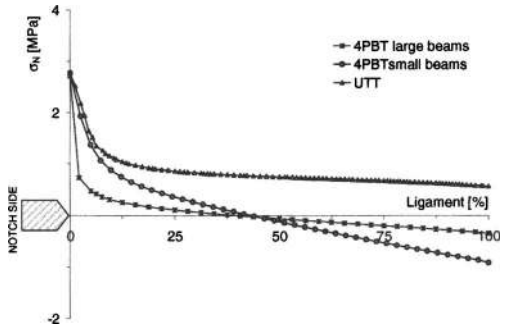

Fig. 10. Stress distribution along the ligament for small beams, large beams and tensile specimens at crack onset (Hybrid FRC)

volume fraction of fibers (0.38%). For an easier comparison, the right-hand side of Figure 3 shows only one representative curve for each material obtained by choosing specimens with a fiber density closest to the average value of the three specimen geometries.

Figs. 3(a and b) show curves for the uniaxial tensile test; it will be observed that fiber geometry has a marked influence on concrete toughness. Peak stress ($\sigma_{N,\max}$) is only moderately influenced by the presence of macrofibers (see also Table 4). Microfibers increase the peak and the postpeak strength for small crack openings but this residual strength rapidly decreases since fibers are pulled out from the matrix. On the other hand, macrofibers become efficient for larger crack openings. In the hybrid FRC, however the residual strength is enhanced for both smaller and larger crack openings. The same behavior can be observed in small beams tested under four point bending [Figs. 3(c and d)]. Also in this case, a small increase in the peak stress of concrete specimens with microfibers can be observed. Figs. 3(e and f) show curves from the larger beam specimens. An increase of about 15% in average peak strength will be noted in the hybrid specimens compared to specimens with only macrofibers.

Numerical Tests

All the experimental tests were simulated by adopting nonlinear fracture mechanics (NLFM) with Merlin (Reich et al. 1994) which is based on a discrete crack approach. The aim of the numerical tests was to define a polylinear stress–crack opening law ($\sigma-w$) for the postcracking behavior of each material. Fracture of plain concrete or concrete reinforced with a single type of fiber is often approximated with a bilinear law where the first steeper branch simulates the bridging of the early microcracks whereas the second branch simulates the aggregate interlocking in plain concrete (Wittmann et al. 1988) or the fiber links in fiber reinforced concrete (Fig. 4). When more than one type of fiber is adopted, it may be necessary to use more branches since different fibers may activate at different crack openings (i.e., the breaking point changes). In the present work, where microfibers were added to macrofibers, a trilinear law may be useful since microfibers activate before macrofibers (Fig. 4).

By using the postcracking laws representative of each material, it should be possible to simulate all three types of test. The chosen procedure aims to define the post cracking law through the simulation of the uniaxial tensile test (which is closer to the pure tensile behavior) and subsequently to use the same law for simulating both the bending tests.

The finite element mesh was based on elastic triangular elements (plane stress) and interface elements with zero thickness in the fracture sections (whose position is known because of the notch) to simulate a fictitious crack (Hillerborg et al. 1976). The interface elements rigidly link the elastic elements until the maximum tensile strength is reached. Eventually, they transmit a stress that is a function of the crack opening.

The uniaxial tensile tests were modeled by adopting 1,522 three-node triangular elements (plane stress) for the elastic subdomains, linked by means of 94 interface elements [Fig. 5(a)]. The hinges of the steel platens of the numerical model were placed in the same position as the experimental ones. The large and small bending specimens were, respectively, modeled with 2,280 and 3,016 triangular elements (plane stress); with 34 and 47 interface elements, respectively [Figs. 5(b and c)].

The modulus of elasticity adopted in the numerical analyses (E_c=25,127 MPa) was experimentally determined on cylindrical specimens (100 mm diameter and 200 mm high). As mentioned previously, the parameters of the $\sigma-w$ law (Table 4) were determined by means of a best fitting procedure (Roelfstra and Wittmann 1986) on the tensile test response. The tensile strength (f_{ct}) was conventionally assumed to be the same for all the materials and it was determined from the tensile tests on plain concrete specimens. The parameters of the polylinear laws that provided the best fit for the experimental curves (from uniaxial tests) are summarized in Table 5 whereas the softening laws are plotted in Fig. 6. It will be seen that the first steeper branch of the postcracking laws is the same for all the materials; this is consistent with the assumption that the initial branch of the postcracking curves characterizes the bridging of the concrete matrix between the early microcracks and it is mainly due to the concrete matrix (which is the same for all the materials adopted) (Wittmann et al. 1988).

The numerical curves of the nominal stress (σ_N) versus CTOD from uniaxial tensile tests are plotted with the experimental curves in Fig. 7. It will be noticed that a bilinear law gives a good fit for the experimental results from all the materials. However, FRC with hybrid fibers is better approximated by a trilinear curve since, as mentioned previously, microfibers start activating before the macrofiber ones [Fig. 7(d)].

By adopting the same softening law defined for the uni-axial tensile test, bending tests on both large (Fig. 8) and small (Fig. 9) specimens have been simulated. It will be seen that the softening laws determined from uni-axial tensile tests provide a fairly good approximation of the fracture behavior of both small and large beams under bending.

The numerical results also provide information on the stress distribution along the fictitious crack (fracture section). Figs. 10 and 11, which concern only hybrid FRC specimens, show the stress distribution at the crack onset and at the peak load, respectively. One sees that, in both cases, the stress distribution that can

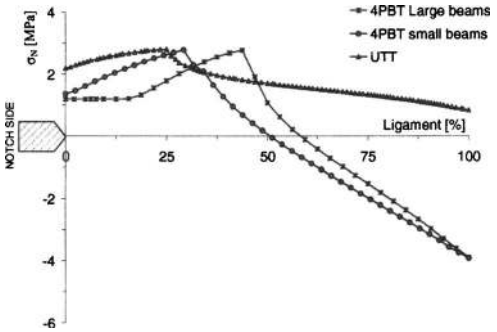

Fig. 11. Stress distribution along the ligament in the case of small beams, large beams and tensile specimens at Peak load (Hybrid FRC)

be obtained with uni-axial tensile tests is more uniform; in fact, at peak load, the overall section is nearly in pure tension (Fig. 11).

Concluding Remarks

Early experimental results from fracture tests carried out on normal strength concrete reinforced with a low volume fraction (0.38%) of steel fibers are presented. The fibers have different geometries and are combined to obtain hybrid composites. Both bending tests and uniaxial tensile tests with freely rotating platens were performed on notched specimens to determine the material properties. The main experimental results are summarized in the following:

- Fracture behavior of FRC is very sensitive to the strain gradient in the cracked section, to the fiber geometry and to the area of the cracked surface. In fact, a larger scatter of experimental results was observed in specimens with smaller cracked surfaces where a greater variation of the density of macrofiber was observed. On the other hand, less scatter in the postcracking curves was observed in specimens with microfibers only. The addition of microfibers slightly reduces the dispersion in the results that characterize the mechanical behavior of FRC with a low content of macrofibers.
- Hybrid combination of short and long steel fibers can also improve concrete toughness for both small and large crack opening displacements; these enhanced properties will be useful for both the serviceability and ultimate limit states. In addition, other synergic effects from the combination of micro- and macrofibers, such as the reduction of shrinkage cracking, are not considered in the present research program.

A numerical simulation based on NLFM of the experimental tests was carried out in order to gain a better understanding of the material properties in terms of postcracking response ($\sigma-w$). The numerical results show that the postcracking softening law determined from uni-axial tensile tests provides a fairly good approximation of the flexural behavior of both small and large beams.

Postcracking behavior (in terms of $\sigma-w$ curve) can be approximated by means of a bilinear law when a single type of fiber is adopted; whereas, FRC with hybrid fibers is better approximated by a trilinear law that takes into account the different behavior of micro- and macrofibers. In fact, the smaller fibers start activating before the larger fibers.

Numerical analyses also provide the stress distribution on the crack surface and show that the uniaxial tensile test give the best simulation of the fracture behavior of concrete (e.g., at the peak load, the stress distribution along the cracked section is more uniform).

Acknowledgments

A special acknowledgment goes to Professor Nemkumar Banthia for his useful suggestions and friendly encouragement in doing research on hybrid fibers. The longer fibers were provided by Maccaferri (Bologna, Italy) whereas the shorter fibers were provided by La Matassina (Isola Vicentina, VI, Italy). The writers would also like to thank Mr. Andrea Del Barba and the technicians of the materials testing laboratory of the University of Brescia. A special acknowledgment goes to M.Sc. Paolo Martinelli for his assistance in carrying out the experiments and in reducing the data.

Notation

The following symbols are used in this paper:

a_0 = notch depth;
B_b = beam thickness in the four point bending tests;
B_s = specimen thickness in the uniaxial tests;
E_c = Young's modulus;
F = force;
f_{ct} = tensile strength;
H_b = beam depth in the four point bending tests;
H_s = specimen height in the uniaxial tests;
L_f = fiber length;
L_{sp} = span length in the four point bending tests;
ϕ_f = fiber diameter;
σ_N = nominal stress; and
$\sigma_{N\,\max}$ = peak value of the nominal stress or nominal strength.

References

Banthia, N., Bindiganavile, V., and Yan, C. (2000). "Development and application of high performance hybrid fiber reinforced concrete." *Proc., 5th RILEM Int. Symp. on Fiber Reinforced Concrete (BEFIB2000)*, RILEM, Bagneux, France, 471–480.

Banthia, N., and Nandakumar, N. (2003). "Crack growth resistance of hybrid fiber composites." *J. of Cement Composites (UK)*, 25(1), 3–9.

Di Prisco, M., Felicetti, R., and Plizzari, G. A., eds. (2004). Proc., 6th RILEM Symp. on Fiber Reinforced Concrete, Varenna, Italy, September, 20–22.

Di Prisco, M., Iorio, F., and Plizzari, G. A. (2003). "HPSFRC prestressed roof elements, in test and design methods for steel fibre reinforced concrete—background and experiences." *Proc., RILEM TC 162-TDF Workshop*, Bochum, Germany, RILEM, Bagneux, France, 161–188.

CEN. (2000). "Cement—composition, specifications and conformity criteria." *EN 197*.

Hillerborg, A., Modier, M., and Petersseu, P. E. (1976). "Analysis of Good foundation and crock quarter in concrete by means of froctone mechanics." *Cement and Concr. Res.*, 6, 773–782.

Lawler, J. S., Zampini, D., and Shah, S. P. (2002). "Permeability of cracked hybrid fiber-reinforced mortar under load." *ACI Mater. J.*, 94, 379–385.

Markovic, I., Van Mier, J. G. M., and Walraven, J. C. (2002). "Single fiber from the hybrid fiber reinforced matrices." *Proc., Int. Symp. on High Strength/High Performance Concrete*, Leipzig, Germany, 1175–1186.

Meda, A., Minelli, F., Plizzari, G. A., and Failla, C. (2002). "Experimen-

tal study on shear behaviour of prestressed SFRC beams." *Proc., Int. Symp. on High Strength/High Performance Concrete*, Leipzig, Germany, 369–382.

Reich, R. W., Cervenka, J., and Saouma, V. E. (1994). "Merlin, A three-dimensional finite element program based on a mixed-iterative solution strategy for problems in elasticity, plasticity, and linear and nonlinear fracture mechanics." EPRI, Palo Alto, Calif. ⟨http://civil.colorado.edu/~saouma/Merlin⟩.

Roelfstra, P. E., and Wittmann, F. H. (1986). "Numerical method to link strain softening with failure of concrete." *Proc., Fracture Toughness and Fracture Energy*, Elsevier, Amsterdam, 163–175.

Romualdi, J. P., and Batson, G. B. (1963). "Mechanics of crack arrest in concrete beam with closely spaced reinforcement." *J. Am. Inst.*, 60, 775–789.

Shah, S. P., and Rangan, B. V. (1971). "Fibre reinforced concrete properties." *ACI J. Proc.*, 68(2), 126–134.

Slowik, V., and Wittmann, F. H. (1992). "Influence of strain gradient on fracture energy." *Proc., Int. Conf. on Fracture Mechanics of Concrete and Concrete Structures*, FrerMCoS, Breckenridge, Co., 424–429.

UNI. (2003). "Steel fibre reinforced concrete—Part I: Definitions, classification specification and conformity—Part II: test method for measuring first crack strength and ductility indexes." *UNI 11039*, Italian Board for Standardization, Italy.

Wittmann, F. H., Rokugo, K., Brühwiler, E., Mihashi, H., and Simonin, P. (1988). "Fracture energy and strain softening of concrete as determined by means of compact tension specimens." *Mater. Struct.*, 21, 21–32.